A Journal of the Gesellschaft Deutscher Chemiker

Angewandte International Edition GDCh Chemie

www.angewandte.org

Accepted Article

Title: Double Exchange Induced in situ Conductivity in Nickel Based Oxyhydroxides: An Effective Descriptor for Electrocatalytic Oxygen Evolution

Authors: Bailin Tian, Hyeyoung Shin, Shengtang Liu, Muchun Fei, Zhangyan Mu, Cheng Liu, Yanghang Pan, Yamei Sun, William A. Goddard III, and Mengning Ding

To be cited as: *Angew. Chem. Int. Ed.* 10.1002/anie.202101906

Link to VoR: https://doi.org/10.1002/anie.202101906

WILEY-VCH

10.1002/anie.202101906

WILEY-VCH

RESEARCH ARTICLE

Double Exchange Induced *in situ* Conductivity in Nickel Based Oxyhydroxides: An Effective Descriptor for Electrocatalytic Oxygen Evolution

Bailin Tian[a]†, Hyeyoung Shin[b],[c]†, Shengtang Liu[a], Muchun Fei[a], Zhangyan Mu[a], Cheng Liu[a], Yanghang Pan[a], Yamei Sun[a], William A. Goddard III*[b] and Mengning Ding*[a]

[a] Bailin Tian, Muchun Fei, Shengtang Liu, Zhangyan Mu, Cheng Liu, Yanghang Pan, Yamei Sun, Prof. Dr. Mengning Ding
Key Laboratory of Mesoscopic Chemistry, School of Chemistry and Chemical Engineering, Nanjing University, Nanjing 210023, China
E-mail: mding@nju.edu.cn
[b] Prof. Dr. Hyeyoung Shin, Prof. Dr. William A. Goddard III
Materials and Process Simulation Center (MSC) and Joint Center for Artificial Photosynthesis (JCAP), California Institute of Technology, Pasadena, California 91125, United States
E-mail: wag@caltech.edu
[c] Prof. Dr. Hyeyoung Shin
Graduate School of Energy Science and Technology (GEST), Chungnam National University, Daejeon 34134, Korea
†These authors contribute equally to this work.

Abstract: The electrocatalytic oxygen evolution reaction (OER) plays an important role in sustainable energy conversion from water to hydrogen fuel. The most effective non-noble metal catalyst for OER is currently Fe-doped NiOOH ($Ni_{1-x}Fe_xOOH$), but its overpotential (theoretically calculated $\eta = 0.4$) is too large for practical applications. Motivated by our *in silico* predictions that Ir dopant would lead to a very low overpotential to improve OER activity of Ni-based hydroxides, we report here an experimental confirmation on the altered OER activities for a series of metals (Mo, W, Fe, Ru, Co, Rh, Ir) doped into γ-NiOOH. Most interestingly, we observed that the *in situ* (intermediate) electrical conductivity for metal doped γ-NiOOH correlates well with the trend in enhanced OER activities. This correlation allows experimental screening of new candidates with fast measurements of intermediate conductivity, while also providing additional information about the catalytic mechanism. To understand the basis of this correlation, we used density functional theory (DFT) calculations to explain the *in situ* conductivity of the key intermediate states of metal doped γ-NiOOH during OER. The simultaneous increase of OER activity with *in situ* conductivity was rationalized by their intrinsic connections to the radical character promotion in the metal-oxo bond. This electrical transport characteristic, which was later linked to the double exchange (DE) interactions between adjacent metal ions with various *d* orbital occupancies, serves as an effective indicator for the key metal-oxo radical character, providing a facile and effective descriptor for the theoretical and experimental guidance in design and screening of efficient OER catalysts.

Introduction

Catalytic water splitting to produce hydrogen and oxygen molecules using solar generated electrical energy is an important step toward sustainable and clean energy. However, in contrast to the hydrogen evolution reaction (HER), the four-electron-proton coupling process for the oxygen evolution reaction (OER) limits the electro-kinetics and efficiency of H_2 production.[1] Extensive research has been reported on development of OER electrocatalysts to reduce the overpotential while improving catalyst stability in specific working environments. To this end, Ni-based oxides and hydroxides materials have been widely used as non-noble metal OER catalysts because of their good catalytic performance in alkaline media.[2] Yet their overpotentials remain considerably too large for energy and cost-efficiency.

Research toward next generation high-performance catalysts relies heavily on information about physical and chemical processes occurring at the catalytic interface during the electro/photo-catalytic conversions, especially under *operando* conditions.[3] Our quantum mechanics (QM) calculations found that the adsorbate evolution mechanism (AEM) applies to OER on IrO_2. Thus water bound to the surface provides an O to the product O_2.[4] Later we used QM calculations to examine the mechanism of OER activity on bare γ-NiOOH and metal doped γ-NiOOH (Fe, Co, Rh, and Ir) and showed that there are 6 important steps for OER as shown in Figure 1, again folllowing AEM.[5]

Here we found that critical for OER on the γ-NiOOH based materials is stabilization of radical character on the oxygen of the metal-oxo bond (M^{IV}-O·) prior to activating an H_2O to form a new O-O bond to the metal (see big dots in states 1 and 4). These studies found a synergistic effect between high spin Fe^{IV} ($3d^4$) stabilizing the M-O radical state and low spin Ni^{IV} ($3d^6$) promoting O-O bond formation. Based on this mechanism, Shin *et al.*[5b] examined 17 possible replacements for the Fe and predicted that replacing Fe with Co, Rh and Ir as dopants in γ-NiOOH would further enhance the OER catalytic activity of γ-$Ni_{1-x}M_xOOH$. In particular Ir was predicted to have greatly improved performance. Our research on (Ni,Fe)OOH concluded that Hybrid DFT (B3PW91) leads to higher accuracy than straight PBE-D3,[5a] we later showed for single crystal nanoparticles of Co doped TiO_2 (where only a single surface facet is exposed) that PBE-D3 leads to turn-over-frequencies as a function of applied potential in excellent agreement with experiments.[6] Thus we use this same level of DFT for the four cases considered here.

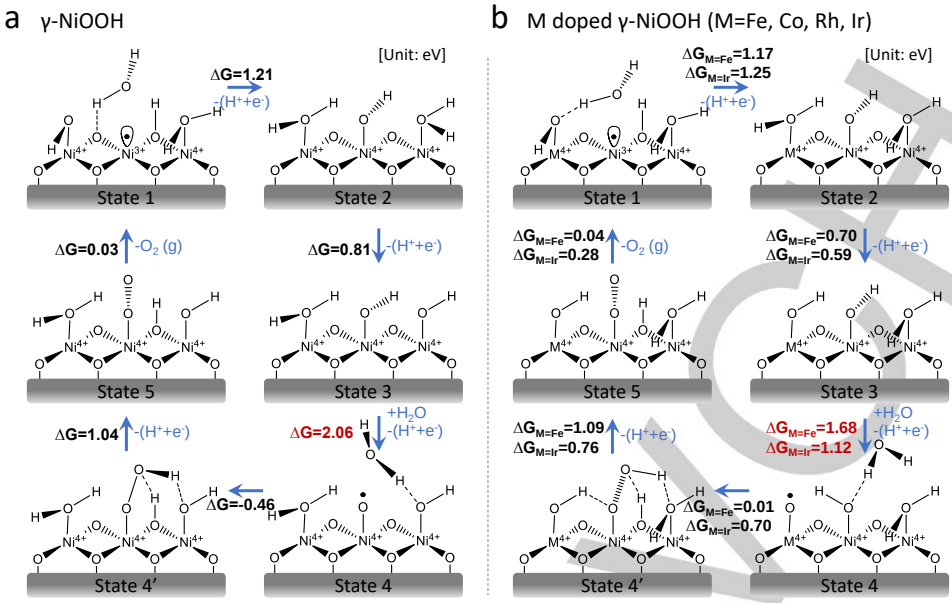

Figure 1. Mechanism for OER on (**a**) bare γ-NiOOH, and (**b**) metal (M) doped γ-NiOOH (M = Fe, Co, Rh, and Ir) catalyst from our previous studies.[5b]

We decided to carry out experiments to validate these exciting catalytic predictions, with an additional goal of finding other characterizations to help provide further mechanistic understanding. Spectroscopic methods such as synchrotron X-ray absorption spectroscopy (XAS)[7] and electron paramagnetic resonance (EPR) spectroscopy[8] can be applied to measure the electronic configuration and spin states for electrocatalytic metal ions. However, these techniques require high-end facilities and are technically challenging. Therefore, we want to develop other simpler techniques to more quickly reveal the *d* orbital occupancy and electron spin states of transition metal ions in situ to help identify promising oxyhydroxide-based OER activities.

In this study, we systematically synthesized a series of metal (Fe, Ru, Co, Rh, Ir, Mo and W) doped NiOOH electrocatalysts with controllable crystal phases using a solvothermal method. An on-chip strategy[3a, 9] was employed to simultaneously obtain both electrochemical cyclic voltammetry (CV) and the operando electrical conductivity of the electrocatalysts. We identified an insulator-to-semiconductor/metal phase transition of the γ-phase Ni-based hydroxide along with the two sets of redox peaks prior to OER at room temperature, providing direct validation to the previous DFT predictions.[10] Importantly, **the OER activity of the metal doped γ-NiOOH showed a positive correlation with their *in situ* conductivity**. We further showed that the potential drop caused by the internal resistance accounted for only a small part of the observed overpotential. Finally, by combining the electrochemical results, *in situ* electrical transport information, and DFT calculations, we established for the first time a relationship between OER activity (mechanism) of Ni-based oxyhydroxides, electronic configuration and spin state of the doped transition metal ions, and the *in situ* (intermediate) conductivity of the electrocatalysts. This work provides solid experimental evidence to establish effective theoretical guidance (synergetic catalytic effect) for design of more efficient OER catalysts using a convenient indicator (double exchange interaction) to estimate OER mechanisms and performance.

Results and Discussion

To reveal the *in situ* information of Ni hydroxides during OER, we successfully synthesized the phase-controllable α-$Ni(OH)_2$, β-$Ni(OH)_2$ using a simple method[11] and γ-NiOOH through precipitation-oxidation approach[12]. The X-ray diffraction (XRD) patterns (Fig. S5a-b) support the formation of pure hexagonal α-$Ni(OH)_2$ (JCPDS #38-0715) and hexagonal β-$Ni(OH)_2$ (JCPDS #14-0117) phases, while the γ-NiOOH does not exhibit a regular crystalline phase (Fig. S10a) as reported previously.[13]

The experimental setup and the working principle of on-chip CV and *in situ* electrical transport spectroscopy (ETS)[3a, 9] of γ-NiOOH and α-$Ni(OH)_2$ are illustrated in Figure 2a and Figs. S12-S19. As-prepared hydroxides thin films were fabricated into micro-device for the on-chip OER and *in situ* conductance studies in O_2-saturated 1 M KOH (99.999%, electronic grade). To detect the near-equilibrium results before and during OER,[14] the scan rate in this work was kept slow (2 $mV \cdot s^{-1}$) to eliminate variations. Typical results for γ-NiOOH and α-$Ni(OH)_2$ are shown in Fig. 2c-d. Two redox peaks were observed in the CV curves prior to OER, which we ascribe to the Ni^{II}-Ni^{III} and Ni^{III}-$Ni^{III/IV}$ redox processes according to reported results,[12] respectively. The CV of empty Au electrode effectively exclude the interference of Au (Fig. S19). Along with the CV cycles, the initial conductivity of γ-NiOOH and α-$Ni(OH)_2$ are both low before Ni^{II}-Ni^{III} oxidation. As the oxidation reaction initiates and progresses during the positive potential scan, the conductance of γ-NiOOH and α-$Ni(OH)_2$ both increase gradually at first and then surges rapidly prior to the second oxidation, reaching a plateau at the oxidation reaction of Ni^{III}-$Ni^{III/IV}$. At this point the sheet conductance has increased by 150-200% (Fig. 2c-d). When the potential is swept negatively, the sheet conductance decreases with the reduction of $Ni^{III/IV}$ to Ni^{III}. With the majority of $Ni^{III/IV}$ reduced to Ni^{III} (potential scanned negatively to 1.35 V vs. RHE), the sheet conductance drops sharply back to the initial state. The *in situ* conductivity increase/decrease, which

10.1002/anie.202101906

reflects the electrical transport characteristics across the surface (intermediate state), is closely related to the $Ni^{III/IV}$ oxidation/reduction. The high-valence $Ni^{III/IV}$ is also the catalytic active sites towards OER, which is consistent with the conclusion from extended X-ray absorption fine structure (EXAFS) studies.[15]

To the best of our knowledge, it has not been previously reported that two kinds of species can be so clearly distinguished prior to OER in bulk CV or LSV. Combining high-resolution of on-chip electrochemistry with concurrent *in situ* conductivity measurements, our micro-device-based technology provides potentially useful high-resolution and comprehensive analysis for these electrocatalytic systems. The CV and ETS results confirmed the equality of α-γ phases, consistent with Bode's mode[16] in which the conversion of Ni hydroxides follows the α-γ or β-β paths. Compared with α phase, the behavior of the β phase varies significantly. It is clear that the *in situ* conductivity of β-$Ni(OH)_2$ stays relatively low, with no obvious variation during the CV cycles (as shown in Figure 3d). This confirms Bode's mode for the β-β conversion path, while theoretical studies also support the low conductivity for β-β conversion.[17] The distinct electrical conductivity characteristic of γ phase intermediate is further validated by our theoretical calculations (discussed below). The larger interlayer spacing of γ-NiOOH reduces the band gap to form electrically conductive pathways, as electrons transport from Ni^{III} to Ni^{IV} centers.

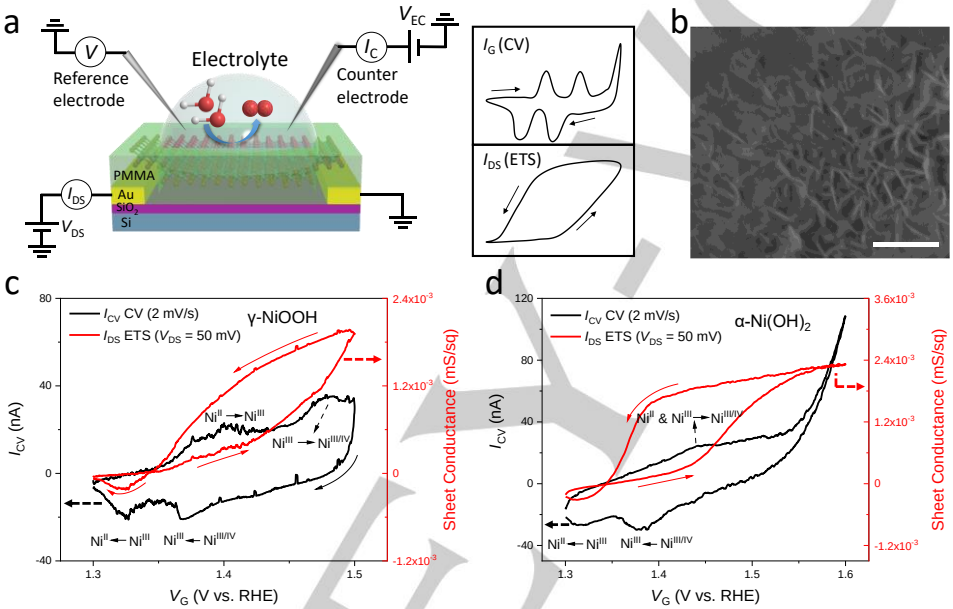

Figure 2. Experimental setup and typical results of on-chip cyclic voltammetry (CV) and electrical transport spectroscopy (ETS) measurement. (**a**) Schematic illustration of the on-chip electrochemical and *in situ* ETS measurements, typical I_G (CV) and I_{DS} (ETS) curves shown on the right. (**b**) Scanning electron microscopy (SEM) image of the assembled α-$Ni(OH)_2$ nanosheet, scale bar is 500 nm. (**c**) I_{CV}-V (on-chip CV, black curve) and I_{DS}−V (ETS, red curve) characteristics of a typical γ-NiOOH device in O_2-saturated 1 M KOH (99.999%, electronic grade). (**d**) On-chip CV (black) and ETS (red) characteristics of a α-$Ni(OH)_2$ device in O_2-saturated 1 M KOH (99.999%, electronic grade). Solid arrows in all figures indicate the potential sweeping direction.

To further study the AEM in Ni-based hydroxides, we introduced a series of dopant elements and systematically evaluated both their OER performance and their *in situ* intermediate conductivities. From the synthetic aspect, it appears that Ni and other first-row transition metals (Fe, Co) tend to form hydroxides (Fig. S5a-b) while Ni and other late transition metals (Mo, W, Ru, Rh, Ir) tend to form intermetallic compounds and face-centered cubic (*fcc*) alloys with surface oxides (Fig. S5c, f). The chemical composition and structure of as-synthesized electrocatalysts were further confirmed by X-ray photoelectron spectroscopy (XPS). The XPS spectra and energy dispersive X-Ray spectroscopy (EDX) in Figs. S7-S9 indicate the successful synthesis of electrocatalysts doped with various metals. For a consistent evaluation of dopant effects in Ni hydroxide-based OER catalysts, all as-prepared samples were pre-oxidized with CV cycles (to a stabilized state) to ensure hydroxide formation on the surface,[18] and we confirmed that significantly higher *in situ* conductance originates from intermediate γ-phases. The additional evidence of hydroxide formation is provided in Figs. S21-S25 and Figs. S35-S36.

The CV and ETS results of $Ni_{0.9}M_{0.1}OOH$ with various doping elements are summarized in Figure 3, where the structures and oxidation states of the active intermediates are shown also for reference according to the *in silico* simulation.[5] Importantly, the OER performance of the electrocatalysts doped with different elements correlates well with our theoretical predictions for γ-phase intermediates, with outstanding performance for Ir.[5b] In addition, while β-$Ni_{0.9}Fe_{0.1}(OH)_2$ has the best catalytic performance among the β phase samples, α-$Ni_{0.9}Fe_{0.1}(OH)_2$ shows an abnormal OER activity (close to pure α-$Ni(OH)_2$, contradictory to our prediction and literature reports for Fe doping), presumably due to synthetic issues that cause unfavorable surface characteristic[19] and/or variations in the electronic configuration. To this end, three alternative approaches (hydrothermal[7d], electro-deposition[20] and ion-exchange[21]) were further employed to prepare $Ni_{0.9}Fe_{0.1}$ hydroxides. All three samples expectedly lead to enhanced OER activities (Fig. 3a and Fig. S33), among which α-$Ni_{0.9}Fe_{0.1}(OH)_2$ prepared *via* ion-exchange approach (the other two resulted in LDHs) demonstrates high *in situ* intermediate conductivity that matches to the observed trend. Overall, it is clear that the *in situ* electrical

10.1002/anie.202101906

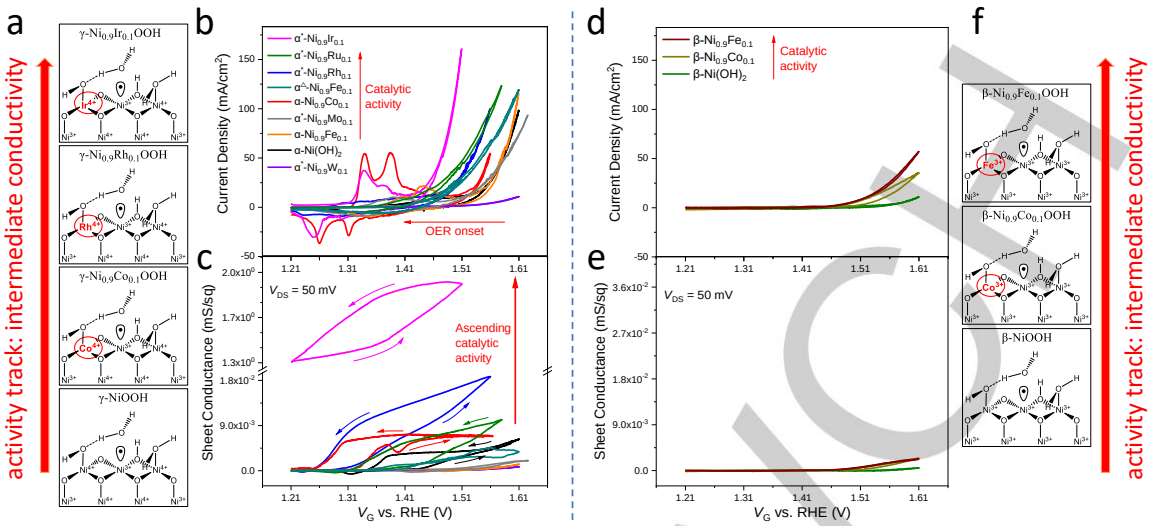

Figure 3. Summary of CV and ETS results for γ and β phase NiOOH for various dopants. (**a**) The expected structures and oxidation states of γ phase intermediates. (**b**) The OER catalytic performance (CV) of α phase and $Ni_{0.9}M_{0.1}$-O_x (M = Mo, W, Ru, Rh, Ir) samples, results are consistent with our theoretical predictions. (**c**) Corresponding *in situ* sheet conductance (ETS) of the various electrocatalysts in (**b**). (**d**) The OER catalytic performance (CV) of β phase samples. (**e**) Corresponding *in situ* sheet conductance (ETS) of the various electrocatalysts in (**d**). (**f**) The expected structures and oxidation states of β phase intermediates. Red arrows in **a** and **f** indicate the trend that higher conductivities lead to lower overpotentials. "α*" in **b** denotes pre-oxidation with CV cycles to achieve α-hydroxide formation on the surface. "α^{Δ}" denotes α-$Ni_{0.9}Fe_{0.1}$ sample prepared through ion-exchange.

conductivity of the γ phase intermediates is generally much higher than that of the β phase, which is partly associated with the Ni^{III}-$Ni^{III/IV}$ oxidation (formation of catalytic active sites and intermediate states with unique electronic structures), as this OER related phase transition does not occur in the β phase.

Comparing the catalytic activities with the *in situ* conductivities representing the transport characteristics of intermediate states of the catalysts, we see that the OER activities from metal doped NiOOH (in both γ and β phases) demonstrate a clear positive correlation to their *in situ* intermediate conductivities. As summarized in Figure 4a, a linear correlation was observed between the *in situ* conductivity (in log scale) and the overpotentials at large current density (50 mA/cm^2). **This interesting trend indicates a potential decisive factor and useful indicator (*in situ* intermediate conductivity) that links to *operando* chemical/physical details and overall catalytic performance, through a relatively simple transport measurement.** In addition, the potential for the dramatic conductivity increase exactly matches with the potential for the second oxidation peak (Ni^{III}-$Ni^{III/IV}$ oxidation), as shown in Fig. 2-3 (also see Table S1 for summary). Indeed, for the high catalytic activity samples like γ-$Ni_{0.9}Rh_{0.1}OOH$ and γ-$Ni_{0.9}Ir_{0.1}OOH$, the active intermediates are usually generated at a less positive potential and the inflection (turn-on) point of the conductance curves appears at lower potential (Fig. 3b-c). Since the average oxidation state of metal sites during the OER process is highly dependent on the second oxidation level, this observation confirms that the more conductive intermediate surface results from the high-oxidation-state related O containing species that leads to improved OER activity, probably due to 1) better charge transfer efficiency and 2) the specific catalytic enhancement and electronic structure alternation from the doped elements at high oxidation states.[5]

We further investigated the mechanistic connections between electrical conductivity of the γ and β phase intermediates and their corresponding OER performance. The Tafel slopes of all samples shown in Fig. 4b-c indicate they follow a similar AEM mechanism for OER (note that larger interfacial and internal charge transport resistance in the on-chip set-up resulted in a systematic larger Tafel slopes compared to bulk set-up). It is clear that the co-catalysts (Co, Rh, Ir doped γ-NiOOH and Fe doped β-NiOOH) with high intermediate conductivities, low turn-on point in ETS, and low OER overpotentials demonstrate lower Tafel slope, indicating a more favorable kinetic path. Two exception in this series are Fe (ion exchange sample) and Ru doped γ-NiOOH, which showed relatively good OER activity but high turn-on potential for conductivity in ETS (Fig. 3b) and the largest Tafel slope (Fig. 4b). Most importantly, all results suggest that intermediate conductivity of both metal doped γ-NiOOH and β-NiOOH is closely and positively linked to the OER electro-kinetics on surface, as summarized in Fig. 4d.

To further study the influence of charge transfer efficiency during the reaction (from operando conductivity), we compared systematically the catalyst *in situ iR* drop and the overpotential for OER, as shown in Fig. 4e and f. In general, catalysts with low intermediate conductance result in a high *iR* drop, which will certainly lead to the increased overpotential for OER (see right top corner in Fig. 4e and f). Similarly, although the β-$Ni_{0.9}Fe_{0.1}OOH$ has the best catalytic performance among β phase electrocatalysts due to the intrinsically active Fe sites,[20, 22] the large internal resistance (*iR*) limits the interfacial charge transfer efficiency (Fig. 4e and f). However, in all catalysts this *iR* drop caused by internal resistance is small compared to the corresponding overpotential (one exception might be α*-$Ni_{0.9}Mo_{0.1}(OH)_2$), indicating that insufficient charge transfer is at least not the single factor for causing the overpotential. Also, the

10.1002/anie.202101906

RESEARCH ARTICLE

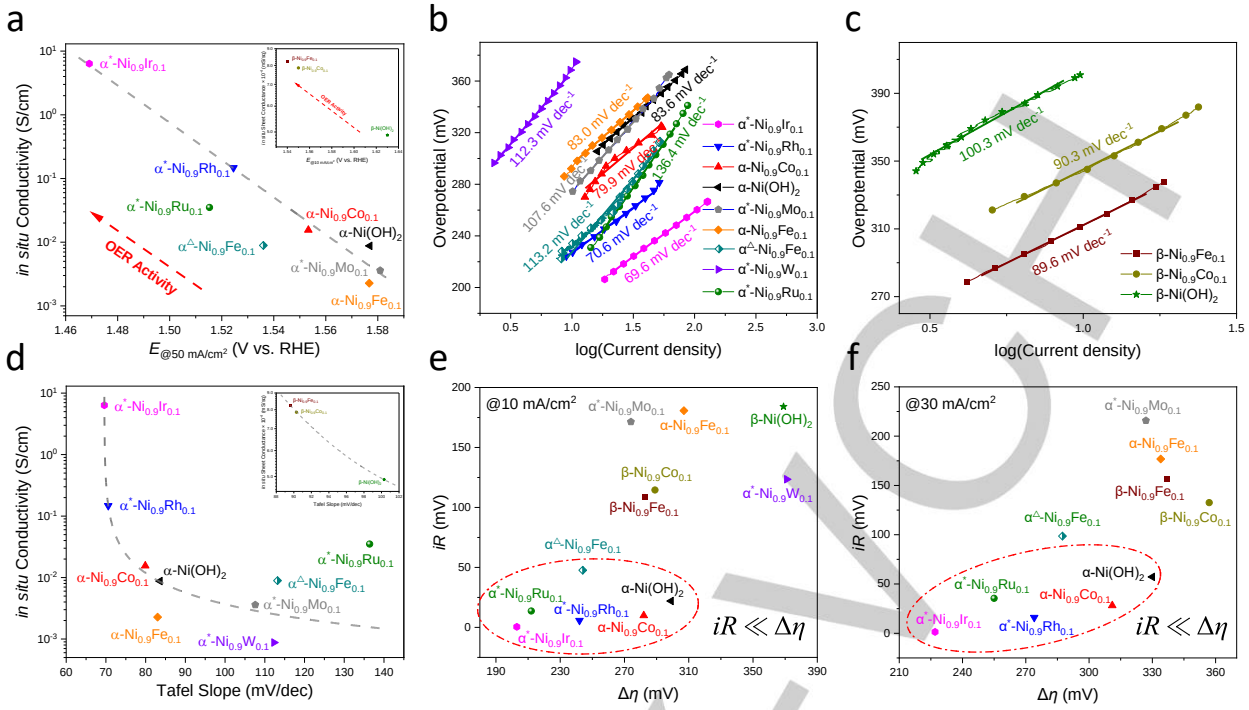

Figure 4. Analysis of the overpotential, Tafel slope, *in situ* conductivity, and *iR* drops of various NiOOH-based electrocatalysts. (**a**) Summary of *in situ* conductivity and OER activity (quantified by the overpotential @50 mA/cm^2) of α and β (inset) phase $Ni_{0.9}M_{0.1}$-OOH. (**b**) Tafel slopes of α phase and $Ni_{0.9}M_{0.1}$-O_x (M = Mo, W, Ru, Rh, Ir) samples. (**c**) Tafel slopes of β phase samples. (**d**) Summary of *in situ* conductivity and Tafel slopes of α and β (inset) phase $Ni_{0.9}M_{0.1}$-OOH. (**e, f**) The comparisons of overpotential Δη and *iR* derived from the *in situ* conductivity (**e**) @10 mA/cm^2, and (**f**) @30 mA/cm^2. It is evident that the potential drop caused by the internal resistance (*iR*) accounts for only a small part of the overpotential (Δη), especially for the catalysts with higher *in situ* conductivity (increased Double exchange interaction), as indicated by dashed cycles in (**e**) and (**f**). "α*" denotes pre-oxidation with CV cycles to achieve α-hydroxide formation on the surface. "α$^\Delta$" denotes α-$Ni_{0.9}Fe_{0.1}$ sample prepared through ion-exchange.

generally suggested p-type doping mechanism arising as a consequence of the "self-gating" effect in the semiconductor OER process[23] **cannot** perfectly explain the trend in $Ni_{0.9}M_{0.1}$-OOH series. This is especially relevant for the generally "good" catalysts with relatively higher intermediate conductivity (such as Co, Rh, and Ir doped γ -NiOOH), where the potential drop caused by the internal resistance accounts for only a negligible part of the observed overpotential (red circles in Fig. 4e and f). Therefore, our conductivity analysis confirms that improved charge transfer efficiency is *not* the main reason for the catalytic enhancement from the effective dopants. Instead, the *in situ* intermediate conductivity should be linked to other factors relevant to specific catalytic enhancements. The CV and ETS results of the catalysts with higher *in situ* conductance and more detailed comparisons of *iR* & Δη can be found in Figs. S29-S32.

Our DFT calculations on the state 4 γ-NiOOH models provide further perspective to rationalize the observed trend in intermediate conductivity of Co group dopants. Figure 5 shows the partial density of state (pDOS) of the key OER intermediates (geometry confirmed in previously studies,[5b] state 4, with the formation of M^{IV}-O·) for γ-NiOOH with Co, Rh and Ir doping, and contributions from each element were clearly separated. The pDOS around E_f reflect the total charge carrier density (at room temperature) and can be linked to the overall metallic conductivity (carrier mobilities can be considered similar in similar intermediate lattices among cobalt group elements doped γ-NiOOH). In addition, the partially filled high-energy anti-bonding orbitals around E_f can induce significant lattice distortion to form small polarons[24] and their intra-layer migration can serve as another electrical transport pathway.[25] It is evident that the total pDOS around Fermi energy (E_f) becomes increasingly larger in the order of pure γ-NiOOH, Co doped, Rh doped, and Ir doped γ-NiOOH from 2.5 to 18.1, which explains the conductance trend observed in the transport measurements. In the band structures of γ-NiOOH based catalytic intermediates, the pDOS around the E_f originates from the π^* anti-bonding in the lattice (contributed by t_{2g} and 2*p* orbitals from M and O atoms, respectively).[26] As shown in Fig. 5, the increased pDOS level around the Fermi level upon Co, Rh and Ir doping results mostly from the increased contribution of the 2*p* orbitals from O·, which also indicates more stabilized radical character upon metal doping.[5] In specific, direct contributions of the Ir *d* orbital is also seen at the E_f (Fig. 5d), which further explains the origin of extraordinary metallic-like conductivity observed in γ-$Ni_{0.9}Ir_{0.1}$OOH (Fig. 3c). Importantly, in contrast to State 4, the pDOS of the following OER intermediates (such as State 4' and State 5, see Figs. S42 and S43) do not exhibit a clear trend that matches to the experimental measurements. We previously concluded that promotion of radical character on the metal-oxo bond (M^{IV}-O·) is essential to increasingly efficient OER as we proceed from Co, to Rh, to Ir.[5b] Similarly, as we predicted previously that the corresponding intermediate ("state 4") is not expected in Ru, Mo and W doped γ-NiOOH (see Fig. S44 for pDOS calculations), the *in situ* measurements indeed revealed the relatively low intermediate conductivities, confirming the different OER mechanisms. The intermediate band structures shown here confirm that, as a direct result of modified pDOS at Fermi level, the ***in situ* intermediate conductivity of a γ-$Ni_{0.9}M_{0.1}$-OOH is an indicator for the high oxidation state of metal and radical character promotion on M^{IV} sites, and therefore the overall OER activities in action**.

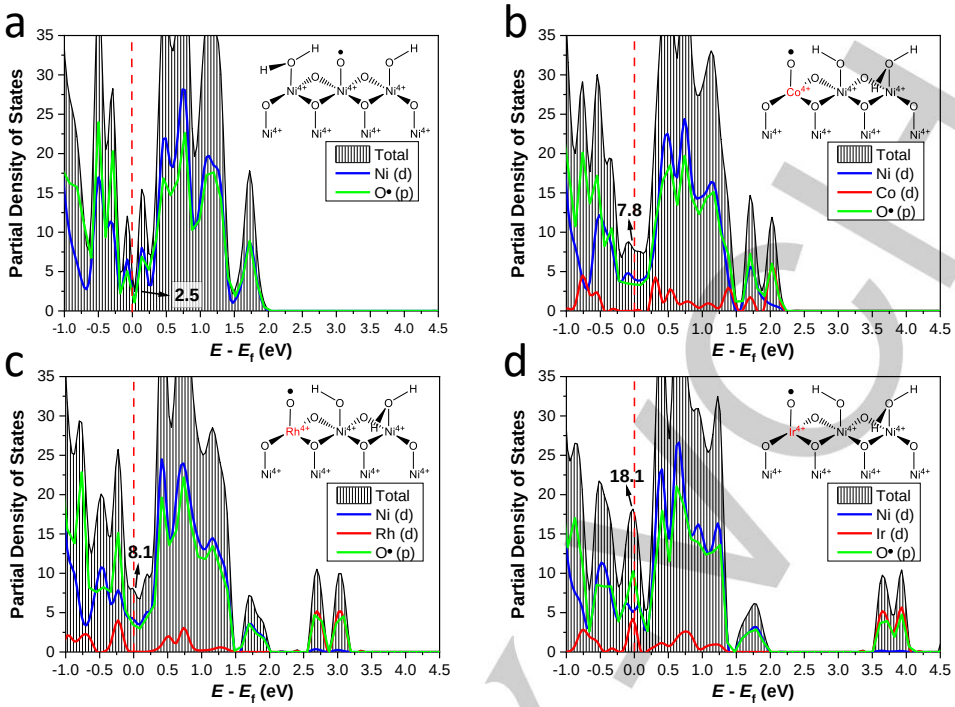

Figure 5. The calculated partial density of state (pDOS) of the key OER intermediates (high energy state 4, with formation of M^{IV}-O·) for γ-NiOOH with Co, Rh and Ir doping. (**a**) The pDOS of γ-NiOOH (State 4 in Figure 1a). (**b**) The calculated pDOS of γ-$Ni_{0.9}Co_{0.1}OOH$ (State 4 in Fig. 1b). (**c**) The calculated pDOS of γ-$Ni_{0.9}Rh_{0.1}OOH$ (State 4 in Fig. 1b). (**d**) The calculated pDOS of γ-$Ni_{0.9}Ir_{0.1}OOH$ (State 4 in Fig. 1b). In each panel, the separate contribution from each element is marked with a distinct color as a visual aid. The position of Fermi energy (E_f) is labelled with red dashed lines for clarity. Chemical structures for each model surface are shown as insets, corresponding to the key OER catalytic step that includes "State 4" acting as the PDS intermediate as previously elucidated.[5b]

To further provide an atomistic understanding of the catalytic mechanism and the detailed electrical conducting mechanism of the γ phase intermediates during OER, the specific electronic configurations (*d* orbital occupancy) of the intermediates were examined. It is known that electron transfer can proceed through oxygen *p* orbitals between adjacent metal ions with different *d* orbital occupancies, leading to conductive pathways through the Double Exchange (DE) interaction, which is generally used to explain the giant magnetoresistance and metallic behavior of manganese perovskite oxides.[27] This phenomenon has also been found in other high valency transition metal oxides.[28] Similarly, models of double exchange transport in the lattice of OER active intermediates are proposed in Figure 6. Due to the empty e_g orbitals and the single hole in the t_{2g} orbitals for $Co^{IV}/Rh^{IV}/Ir^{IV}$ $(t_{2g})^5$, which has been established recently by *in situ* soft XAS measurements,[29] the DE interaction between Ni ions and Co ions *via* oxygen can provide increased *in situ* conductivity of Co group doped γ-NiOOH (illustrated by arrows in Fig. 6b-d). The DE interaction between the e_g orbitals of Ni^{III} and $Co^{IV}/Rh^{IV}/Ir^{IV}$ can also be viewed as a Ni^{3+}–O^{2-}–Ni^{4+} hopping. The DE interaction between t_{2g} orbitals is also possible, in the edge-sharing $Ni_{0.9}M_{0.1}O_6$ (M = Co, Rh, Ir) octahedra, the mostly filled t_{2g} orbitals of $Co^{IV}/Rh^{IV}/Ir^{IV}$ could interact with t_{2g} orbitals of the nearby Ni^{III}, Ni^{IV} and $Co^{IV}/Rh^{IV}/Ir^{IV}$, serving as inherent carrier hopping pathway in the lattice to ensure electrical transport,[30] in good agreement with the *in situ* transport (ETS) results shown in Fig. 3c and the pDOS in Fig. 5b-d. Other theoretical studies also confirm the significance of the partially occupied $(t_{2g})^5$ orbitals near the Fermi level in determining the electronic states and magnetic properties in IrO_2.[26] We now understand the vital role of M^{IV} in the OER catalysis since it both promotes radical character in M^{IV}-O· for the Potential Determining Step (PDS) of OER and leads to the improved *in situ* conductivity through enhanced DE interaction (significantly increased pDOS at E_f). Thus our experimental and theoretical results provide solid evidence validating the theoretical description for the OER mechanisms in terms of $Co^{IV}/Rh^{IV}/Ir^{IV}$ $(t_{2g})^5$ sites and Ni^{IV} $(t_{2g})^6$ sites providing a synergistic catalytic effect to achieve improved catalytic efficiency along with higher *in situ* conductivity (where both Ni and the doped elements obtain high oxidation states and promote the formation of radical characters in metal-oxo bond). Although the *d* orbital occupancy is derived indirectly (*in situ* conductivity and *in silico* simulation), our experimental apparatus provides valuable *operando* information, and is easy to apply. Therefore, *in situ* conductivity provides a facile, efficient and supplementary on-chip method to support the results drawn by spectroscopic methods such as XAS and EPR spectroscopy, and provides useful insights to understand the *in silico* predictions.

10.1002/anie.202101906

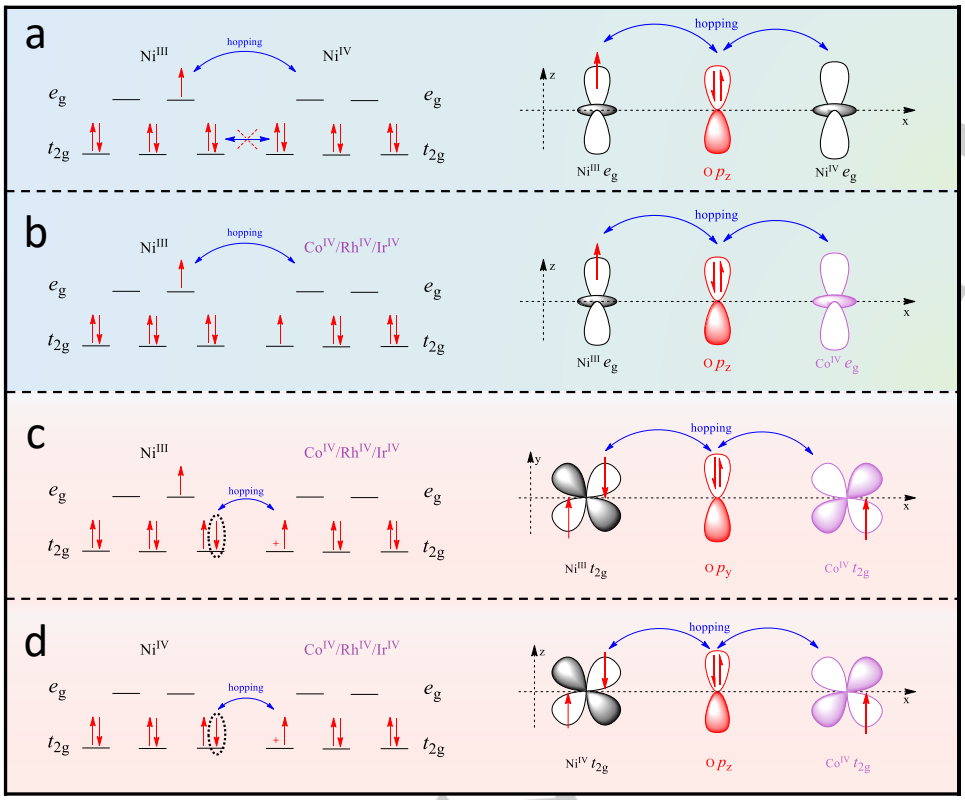

Figure 6. Schematic illustration of the double exchange (DE) interaction and the resulting conductive pathways in the γ phase lattice. (**a, b**) Illustration of possible DE interaction of e_g orbitals between Ni^{III} and Ni^{IV} (**a**), Ni^{III} and $Co^{IV}/Rh^{IV}/Ir^{IV}$ (**b**). (**c-d**) Illustration of possible DE interaction (or hopping pathway) of t_{2g} orbitals between Ni^{III} and $Co^{IV}/Rh^{IV}/Ir^{IV}$ (**c**), Ni^{IV} and $Co^{IV}/Rh^{IV}/Ir^{IV}$ (**d**). The left part in all of the figures is the *d* orbital occupancy of two adjacent metal ions, the right part is the DE interaction, and the spatial orientation of *d* orbitals is also taken into consideration.

On these fundamental basics, the catalysts (Co, Rh, Ir doped γ-NiOOH) showing synergetic catalytic effects have strong DE interaction (higher *in situ* conductance), leading to relatively low overpotential and small Tafel slope. Catalysts (such as Ru doped γ-NiOOH) with only moderate exchange interactions (see Fig. S36) can lead to a relatively lower overpotential but with slow kinetics (probably through a different catalytic mechanism).[5b] In Fe doped cases, the high OER activity and low *in situ* conductivity of NiFe-LDHs (by hydrothermal and electro-deposition preparation, see Fig. S33) can be explained by their distinct OER mechanism. It was reported that the active OER site in Fe-based LDHs is Fe^{III} rather than Ni-Fe[7c, 31]. Therefore, the lack of high covalency (high oxidation states, Ni^{IV}) and nonexistence of Fe^{IV}-O· together resulted in low *in situ* conductivity. The behaviors of α^{Δ}-$Ni_{0.9}Fe_{0.1}$-$(OH)_2$ (by ion exchange preparation) exhibited high *in situ* conductivity that matches to the trend in catalytic activity. Additionally, it can be noted in Fig. 4a that α^{*}-$Ni_{0.9}Ru_{0.1}(OH)_2$ and α^{Δ}-$Ni_{0.9}Fe_{0.1}(OH)_2$ show a slight shift to the linear correlation in Ir, Rh, Co, and pristine cases, which can be rationalized by the previous prediction that radical promotion mechanism exists in Ir, Rh, Co cases but not in Ru, Mo, and W cases. In α^{Δ}-$Ni_{0.9}Fe_{0.1}(OH)_2$ case, the mechanism is more complicated, which may involve the combination/competition between two mechanistic pathways. For catalyts with low *in situ* conductivity (Mo, W doped γ-NiOOH and β-NiOOH), their transport characteristics indicate the lack of DE interaction (although theoretically possible, see Figs. S38-40) and thus different OER mechanism[32], which are not good candidates for OER due to the large *iR* and slow kinetics.

To provide additional experimental confirmation, we further investigated the pH dependence in CV & ETS tests (see Fig. S41). Results show that the OER activity of γ-$Ni_{0.9}Rh_{0.1}OOH$ has a strong pH-dependence, with better catalytic performance and higher *in situ* conductance observed at higher pH values. These data further confirm the importance of the oxidation state of doped metals. When it is more difficult to oxidize the transition metal to a high oxidation state to form active O containing intermediates (State 4) at neutral pH, the consequence is weak DE interaction in the intermediate structure leading to low *in situ* conductance and large OER overpotential. For alkaline media with high pH, the large number of γ-phase intermediates (state 4) generated at lower potential and the enhanced DE interactions lead to higher *in situ* conductance and better catalytic activity. Thus, we further confirmed that **DE-induced transport characteristic in Ni-based oxyhydroxides strongly correlates to the oxidation states and *d* orbital occupancies of transition metal ions**, which are crucial towards the formation of OER active "state 4" intermediate structure, the promotion of radical character in the metal-oxo bond (M^{IV}-O·), and consequent OER performance. In addition to the Ni-based oxyhydroxides, DE interaction has been recently proposed to boost the OER performance in other systems such as spinel oxides.[33] Moreover, spectroscopic studies also suggested the surface reconstructed oxyhydroxides

to be a general intermediate OER active phase in metal nitrides,[18b] spinel oxides and perovskites,[34] metal-organic frameworks,[35] where internal DE interaction might also exist and contribute to the OER activity. Therefore, the DE-induced transport indicator, enabled by on-chip *in situ* measurements demonstrated in this work, can potentially help elucidate the OER mechanisms in various classes of inorganic materials, where the mixed valence metal oxyhydroxide plays an essential role in the electro-oxidative process. This certainly calls for ongoing and systematic investigations in future.

Conclusions

In conclusion, by combining on-chip CV, *in situ* intermediate conductance measurements, and DFT analysis of Ni-based OER electrocatalysts, we demonstrate that double exchange (DE) interactions within the intermediate surface lattice can be strongly related to the catalytic performance and used to elucidate the reaction mechanisms. The catalysts (Co, Rh, Ir doped γ-NiOOH) with strong exchange interaction and radical character promotion in metal-oxo bond (indicated by higher *in situ* conductance) lead to favorable OER thermodynamics (lower overpotentials) and electro-kinetics (smaller Tafel slopes). We have established the relationships between catalytic activity, *d* orbital electronic configuration, and *in situ* conductivity for intermediates in OER electrocatalysts. We conducted related studies directly from catalytically active intermediates and successfully obtained *operando* information for electrocatalytic reactions. This provides practical theoretical guidance for the design of more efficient OER catalysts using atomistic reaction mechanisms. Furthermore, the on-chip methodology and the identified DE-induced transport indicator are expected in the future investigations on other inorganic systems sharing similar structural/electronic intermediate details for the electro-oxidative reactions.

Acknowledgements

B.T. and M.D. acknowledge the support by the Fundamental Research Funds for the Central Universities in China (020514380224), and Natural Science Foundation of Jiangsu Province (BK20180321). H.S. and W.A.G. were supported by the US National Science Foundation (CBET-1805022) and the National Research Foundation of Korea (No. 2020R1C1C1008458).

Keywords: oxygen evolution reaction • Ni-based oxyhydroxides • *in situ* intermediates conductivity • active metal *d* orbital • double exchange interaction

[1] a) H. Mistry, A. S. Varela, S. Kühl, P. Strasser, B. R. Cuenya, *Nat. Rev. Mater.* **2016**, *1*, 1-14; b) Z. W. Seh, J. Kibsgaard, C. F. Dickens, I. Chorkendorff, J. K. Nørskov, T. F. Jaramillo, *Science* **2017**, *355*, eaad4998; c) N.-T. Suen, S.-F. Hung, Q. Quan, N. Zhang, Y.-J. Xu, H. M. Chen, *Chem. Soc. Rev.* **2017**, *46*, 337-365; d) H. Mistry, A. S. Varela, S. Kühl, P. Strasser, B. R. Cuenya, *Nat. Rev. Mater.* **2016**, *1*, 16009.

[2] X.-Y. Yu, Y. Feng, B. Guan, X. W. D. Lou, U. Paik, *Energy Environ. Sci.* **2016**, *9*, 1246-1250.

[3] a) M. Ding, Q. He, G. Wang, H.-C. Cheng, Y. Huang, X. Duan, *Nat. Commun.* **2015**, *6*, 1-9; b) K. Xu, P. Chen, X. Li, Y. Tong, H. Ding, X. Wu, W. Chu, Z. Peng, C. Wu, Y. Xie, *J. Am. Chem. Soc.* **2015**, *137*, 4119-4125; c) M. Zhang, M. De Respinis, H. Frei, *Nat. Chem.* **2014**, *6*, 362; d) A. Bergmann, E. Martinez-Moreno, D. Teschner, P. Chernev, M. Gliech, J. F. De Araújo, T. Reier, H. Dau, P. Strasser, *Nat. Commun.* **2015**, *6*, 8625.

[4] Y. Ping, R. J. Nielsen, W. A. Goddard III, *J. Am. Chem. Soc.* **2017**, *139*, 149-155.

[5] a) H. Xiao, H. Shin, W. A. Goddard III, *Proc. Natl. Acad. Sci. U. S. A.* **2018**, *115*, 5872; b) H. Shin, H. Xiao, W. A. Goddard III, *J. Am. Chem. Soc.* **2018**, *140*, 6745-6748.

[6] C. Liu, J. Qian, Y. Ye, H. Zhou, C.-J. Sun, C. Sheehan, Z. Zhang, G. Wan, Y.-S. Liu, J. Guo, S. Li, H. Shin, S. Hwang, T. B. Gunnoe, W. A. Goddard III, S. Zhang, *Nat. Catal.* **2021**, *4*, 36-45.

[7] a) M. W. Haverkort, Z. Hu, J. C. Cezar, T. Burnus, H. Hartmann, M. Reuther, C. Zobel, T. Lorenz, A. Tanaka, N. B. Brookes, *Phys. Rev. Lett.* **2006**, *97*, 176405; b) J. Simböck, M. Ghiasi, S. Schönebaum, U. Simon, F. M. F. de Groot, R. Palkovits, *Nat. Commun.* **2020**, *11*, 1-10; c) M. Görlin, P. Chernev, J. Ferreira de Araújo, T. Reier, S. Dresp, B. Paul, R. Krähnert, H. Dau, P. Strasser, *J. Am. Chem. Soc.* **2016**, *138*, 5603-5614; d) F. Dionigi, Z. Zeng, I. Sinev, T. Merzdorf, S. Deshpande, M. B. Lopez, S. Kunze, I. Zegkinoglou, H. Sarodnik, D. Fan, A. Bergmann, J. Drnec, J. F. d. Araujo, M. Gliech, D. Teschner, J. Zhu, W.-X. Li, J. Greeley, B. R. Cuenya, P. Strasser, *Nat. Commun.* **2020**, *11*, 2522.

[8] a) J. G. McAlpin, Y. Surendranath, M. Dincă, T. A. Stich, S. A. Stoian, W. H. Casey, D. G. Nocera, R. D. Britt, *J. Am. Chem. Soc.* **2010**, *132*, 6882-6883; b) R. I. Sayler, B. M. Hunter, W. Fu, H. B. Gray, R. D. Britt, *J. Am. Chem. Soc.* **2020**, *142*, 1838-1845.

[9] M. Ding, G. Zhong, Z. Zhao, Z. Huang, M. Li, H.-Y. Shiu, Y. Liu, I. Shakir, Y. Huang, X. Duan, *ACS Cent. Sci.* **2018**, *4*, 590-599.

[10] P. Hermet, L. Gourrier, J. L. Bantignies, D. Ravot, T. Michel, S. Deabate, P. Boulet, F. Henn, *Phys. Rev. B* **2011**, *84*, 235211.

[11] M. Gao, W. Sheng, Z. Zhuang, Q. Fang, S. Gu, J. Jiang, Y. Yan, *J. Am. Chem. Soc.* **2014**, *136*, 7077-7084.

[12] L. Liu, Z. Zhou, C. Peng, *Electrochim. Acta* **2008**, *54*, 434-441.

[13] X. Zheng, B. Zhang, P. De Luna, Y. Liang, R. Comin, O. Voznyy, L. Han, F. P. García de Arquer, M. Liu, C. T. Dinh, T. Regier, J. J. Dynes, S. He, H. L. Xin, H. Peng, D. Prendergast, X. Du, E. H. Sargent, *Nat. Chem.* **2018**, *10*, 149-154.

[14] M. J. Natan, D. Belanger, M. K. Carpenter, M. S. Wrighton, *J. Phys. Chem.* **1987**, *91*, 1834-1842.

[15] D. K. Bediako, B. Lassalle-Kaiser, Y. Surendranath, J. Yano, V. K. Yachandra, D. G. Nocera, *J. Am. Chem. Soc.* **2012**, *134*, 6801-6809.

[16] H. Bode, K. Dehmelt, J. Witte, *Electrochim. Acta* **1966**, *11*, 1079-IN1071.

[17] A. J. Tkalych, K. Yu, E. A. Carter, *J. Phys. Chem. C* **2015**, *119*, 24315-24322.

[18] a) B. Wang, K. Zhao, Z. Yu, C. Sun, Z. Wang, N. Feng, L. Mai, Y. Wang, Y. Xia, *Energy Environ. Sci.* **2020**, *13*, 2200-2208; b) J. Huang, Y. Li, Y. Zhang, G. Rao, C. Wu, Y. Hu, X. Wang, R. Lu, Y. Li, J. Xiong, *Angew. Chem. Int. Ed.* **2019**, *58*, 17458-17464.

[19] Y.-F. Li, A. Selloni, *ACS Catal.* **2014**, *4*, 1148-1153.

[20] L. Trotochaud, S. L. Young, J. K. Ranney, S. W. Boettcher, *J. Am. Chem. Soc.* **2014**, *136*, 6744-6753.

[21] Q. Zhou, Y. Chen, G. Zhao, Y. Lin, Z. Yu, X. Xu, X. Wang, H. K. Liu, W. Sun, S. X. Dou, *ACS Catal.* **2018**, *8*, 5382-5390.

[22] a) M. S. Burke, M. G. Kast, L. Trotochaud, A. M. Smith, S. W. Boettcher, *J. Am. Chem. Soc.* **2015**, *137*, 3638-3648; b) S. Lee, L. Bai, X. Hu, *Angew. Chem. Int. Ed.* **2020**, *59*, 8072-8077.

[23] Y. He, Q. He, L. Wang, C. Zhu, P. Golani, A. D. Handoko, X. Yu, C. Gao, M. Ding, X. Wang, F. Liu, Q. Zeng, P. Yu, S. Guo, B. I. Yakobson, L. Wang, Z. W. Seh, Z. Zhang, M. Wu, Q. J. Wang, H. Zhang, Z. Liu, *Nat. Mater.* **2019**, *18*, 1098-1104.

[24] S. P. Ong, Y. Mo, G. Ceder, *Phys. Rev. B* **2012**, *85*, 081105.

[25] a) A. J. Millis, P. B. Littlewood, B. I. Shraiman, *Phys. Rev. Lett.* **1995**, *74*, 5144; b) H. Ju, H.-C. Sohn, K. M. Krishnan, *Phys. Rev. Lett.* **1997**, *79*, 3230.

[26] Y. Ping, G. Galli, W. A. Goddard III, *J. Phys. Chem. C* **2015**, *119*, 11570-11577.

[27] a) C. Zener, *Phys. Rev.* **1951**, *82*, 403-405; b) P. W. Anderson, H. Hasegawa, *Phys. Rev.* **1955**, *100*, 675-681; c) P. G. de Gennes, *Phys. Rev.* **1960**, *118*, 141-154.

[28] a) M. A. Korotin, V. I. Anisimov, D. I. Khomskii, G. A. Sawatzky, *Phys. Rev. Lett.* **1998**, *80*, 4305-4308; b) X. Peng, Y. Guo, Q. Yin, J. Wu, J. Zhao, C. Wang, S. Tao, W. Chu, C. Wu, Y. Xie, *J. Am. Chem. Soc.* **2017**, *139*, 5242-5248; c) L. S. I. Veiga, G. Fabbris, M. van Veenendaal, N. M. Souza-Neto, H. L. Feng, K. Yamaura, D. Haskel, *Phys. Rev. B* **2015**, *91*, 235135; d) J. Li, J. Ma, K. Du, E. Zhao, J. Guo, J. Mao, T. Ling, *Chem. Commun.* **2020**, *56*, 15004-15007.

[29] J. Zhou, L. Zhang, Y.-C. Huang, C.-L. Dong, H.-J. Lin, C.-T. Chen, L. H. Tjeng, Z. Hu, *Nat. Commun.* **2020**, *11*, 1984.

[30] a) M. F. Liu, Z. Z. Du, Y. L. Xie, X. Li, Z. B. Yan, J. M. Liu, *Sci. Rep.* **2015**, *5*, 9922; b) Y. Bitla, Y.-Y. Chin, J.-C. Lin, C. N. Van, R. Liu, Y. Zhu, H.-J. Liu, Q. Zhan, H.-J. Lin, C.-T. Chen, Y.-H. Chu, Q. He, *Sci. Rep.* **2015**, *5*, 15201; c) J. W. Quilty, A. Shibata, J. Y. Son, K. Takubo, T. Mizokawa, H. Toyosaki, T. Fukumura, M. Kawasaki, *Phys. Rev. Lett.* **2006**, *96*, 027202; d) M. Butel, L. Gautier, C. Delmas, *Solid State Ionics* **1999**, *122*, 271-284.

[31] S. Lee, K. Banjac, M. Lingenfelder, X. Hu, *Angew. Chem. Int. Ed.*

10.1002/anie.202101906

2019, *58*, 10295-10299.
[32] a) B. Zhang, L. Wang, Z. Cao, S. M. Kozlov, F. P. García de Arquer, C. T. Dinh, J. Li, Z. Wang, X. Zheng, L. Zhang, Y. Wen, O. Voznyy, R. Comin, P. De Luna, T. Regier, W. Bi, E. E. Alp, C.-W. Pao, L. Zheng, Y. Hu, Y. Ji, Y. Li, Y. Zhang, L. Cavallo, H. Peng, E. H. Sargent, *Nat. Catal.* **2020**, *3*, 985-992; b) L. Wang, Y. Zhu, Y. Wen, S. Li, C. Cui, F. Ni, Y. Liu, H. Lin, Y. Li, H. Peng, B. Zhang, *Angew. Chem. Int. Ed.* **2021**, *60*, 10577-10582.
[33] J. Li, D. Chu, H. Dong, D. R. Baker, R. Jiang, *J. Am. Chem. Soc.* **2020**, *142*, 50-54.
[34] a) T.-H. Shen, L. Spillane, J. Vavra, T. H. M. Pham, J. Peng, Y. Shao-Horn, V. Tileli, *J. Am. Chem. Soc.* **2020**, *142*, 15876-15883; b) J. N. Hausmann, S. Mebs, K. Laun, I. Zebger, H. Dau, P. W. Menezes, M. Driess, *Energy Environ. Sci.* **2020**, *13*, 3607-3619.
[35] S. Zhao, C. Tan, C.-T. He, P. An, F. Xie, S. Jiang, Y. Zhu, K.-H. Wu, B. Zhang, H. Li, J. Zhang, Y. Chen, S. Liu, J. Dong, Z. Tang, *Nat. Energy* **2020**, *5*, 881-890.

10.1002/anie.202101906

WILEY-VCH

RESEARCH ARTICLE

Entry for the Table of Contents

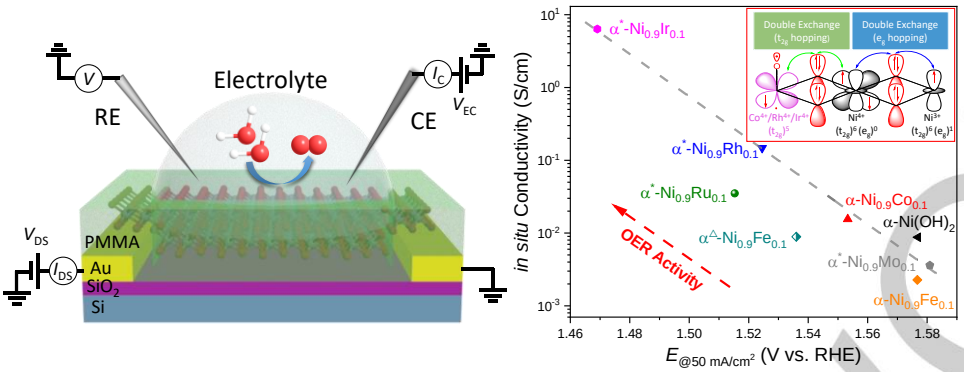

TOC: (left) The on-chip experimental apparatus that allows the concurrent CV and in situ conductivity (ETS) measurements. (right) The correlation between OER activity and *in situ* conductivity at large current density (50 mA/cm^2). Inset illustrates the double exchange (DE) interactions between high valency transition metal ions with different *d* orbital occupancies in the lattice of OER active intermediates containing metal-oxo bond (M^{IV}-O·) can serve as the conductive pathways.